7

Calculation of Long Bone Loading Using Strain Gauges

J. R. Funk and J. R. Crandall

*This paper has not been screened for accuracy nor refereed by any body of scientific peers
and should not be referenced in the open literature.*

ABSTRACT

The standard methodology for measuring loads in long bones is the in situ *load cell, which enables direct measurements, but alters the stiffness and mass of the subject bone. Bone loading can also be calculated by applying linear beam theory to measurements from strain gauges affixed to the bone surface. The efficacy of the strain gauge method was assessed in this study by mounting three strain gauge rosettes to the midshaft of the tibia in two cadaveric above-knee leg specimens. The specimens were subjected to quasistatic axial compression tests, and then the tibia was removed and subjected to four-point bending tests. Linear beam theory for an irregularly shaped cross-section was used to calculate the axial load and bending moments in the tibia. It was possible to accurately calculate the bending moments in the bone, but the calculated axial loads appeared to be grossly in error. The errors in the axial load results could be corrected by calculating an "effective" centroid for each bone, which was found to be approximately 1.5 mm away from the location of the area centroid as determined from CT scans. In spite of the error associated with calculating axial loads, this methodology shows promise for biomechanical experiments in which long bone bending is the parameter of greatest interest and implanting a load cell is problematic (e.g., vehicle-pedestrian tests).*

INTRODUCTION

Measurements of the loads and moments experienced by long bones are often essential data in biomechanical experiments. A common instrumentation technique is to implant a load cell *in situ*, which offers the advantage of direct load measurement in up to six degrees of freedom. However, there are several drawbacks to implanting a load cell; it is an invasive procedure that alters the geometry, stiffness, and mass of the affected bone. Also, any fracture that occurs at the bone/potting interface must be considered artifactual. Artifactual fractures adjacent to hardware mounted to the bone have occurred with high frequency in past studies on axial impacts to the foot (Funk et al., 2002) and lateral impacts to the leg (Kajzer et al., 1997).

Strain gauges offer a much less invasive alternative that maintains the original bone structure. Such instrumentation has been affixed directly to the tibia of human volunteers in one (Lanyon et al., 1975) or two locations (Burr et al., 1996; Ekenman et al., 1998) in order to evaluate physiological loading at a particular site. However, it has long been recognized that strain measurements must be taken at a minimum of three

locations in order to fully characterize the spatial distribution of axial strain across a cross-section (Rybicki et al., 1977; Gross et al., 1992). Investigators have used three or more strain gauges to map out the strain field in a bone cross-section in studies using live animals (Rybicki et al., 1977; Gross et al., 1992; Hartman et al., 1984; Yoshikawa et al., 1994; Gautier et al., 2000; Demes et al., 2001) and human cadavers (Goodwin and Sharkey, 2002). There are two advantages to completely characterizing the strain field of a cross-section. First, peak strains that do not necessarily occur at the location of the strain gauges can be determined. Second, the axial strain field can be decomposed into components attributable to pure axial compression and pure bending. If rosette strain gauges are used, it may also be possible to determine the strain component due to torsion, as well. This information provides more insight into overall bone loading than can be provided by isolated strain measurements at discrete locations.

Long bone loading can be further quantified by calculating the loads and moments experienced by the bone cross-section based on these *in vivo* or *in vitro* strain measurements. The simplest approach is direct calibration, in which pre-test or post-test loading is applied to specimen in an attempt to reproduce the strains measured during testing (Lambert, 1971; Shaaban et al., 2004). This approach is valid so long as the loading applied during the calibration procedure is exactly the same as the loading applied during the test. However, if less than three strain measurements are taken per cross-section, they are not unique. It could be possible to match the strains measured during the test using an entirely different loading regime during the calibration procedure, which would produce misleading results.

A more rigorous and often necessary improvement over the direct calibration approach is to apply beam theory to calculate bone loads and moments from strain measurements. Rybicki et al. (1977) developed a mathematical model based on linear beam theory to calculate axial loading in horse long bones using *in vivo* strain measurements. In this model, the strain field in each bone was decomposed into bending and axial components, and the axial load and bending moments were calculated based on the geometric properties of the cross-section and an assumed elastic modulus. Carter et al. (1981) developed a calibration procedure in which known axial loads and moments were applied to the bone in order to empirically derive an "effective" modulus and "effective" centroid location for the cross-section. This method provides additional accuracy by accounting for error introduced by the assumption that bone material is homogeneous. Some investigators have supplemented analytical beam theory with finite element modeling (Huiskes, 1982; Gross et al., 1992). Huiskes (1982) compared strain measurements in a femur instrumented with 100 strain gauge rosettes to output from a finite element model and concluded that bone behaves as a linear elastic material, and can be treated as an isotropic material for applications in which torsion is not the predominant loading component.

The distribution of loads and moments experienced by the tibia and fibula when the leg is in axial compression has been studied by researchers and clinicians interested in the effects of fibular resection. Although many investigators have studied the human tibia and fibula using strain gauges mounted to three or more locations around a cross-section (Lambert, 1971; Segal et al., 1981; Bourne et al., 1984; Skraba and Greenwald, 1984; Thomas et al., 1995; Wang et al., 1996), none have documented how to calculate the loads and moments experienced by the bone by the proper application of beam theory. The present work is a pilot study conducted to evaluate the efficacy of combining linear beam theory with *in vitro* strain gauge data to calculate the loads and moments experienced by the human tibia when the leg is subjected to axial compression.

METHODS

Two (2) fresh-frozen lower extimities from two different individuals were obtained from medical cadavers in accordance with ethical guidelines and research protocol approved by a University of Virginia Institutional Review Board (Table 1). Prior to testing, the specimens were screened for HIV and hepatitis, and x-rays were checked for signs of pre-existing bone and joint pathology. For each individual, the bone mineral density (BMD) of the mid-diaphyseal portion of the contralateral tibia was determined using dual-energy x-ray absorbtiometry (DEXA). The specimens were sectioned approximately 20 cm above the knee, instrumented, and subjected to a battery of mechanical tests (Table 2).

Table 1. Specimen Information.

Specimen ID	Age (yrs)	Gender	Height (cm)	Weight (kg)	BMD (g/cm^2)	Cause of death
100-L	42	Female	168	71.4	1.208	Acute myocardial infarction
91-R	65	Female	165	64.5	0.861	Cardiac arrest

Table 2. Test Matrix. A-M Refers To The Anteromedial Face Of The Tibia.

Test name	Specimen ID	Loading mode	Specimen orientation	External load	External moment
Ax1a	100-L	Axial load	Knee fully flexed	2000 N	--
Ax1b	100-L	Axial load	Knee flexed 90°	2000 N	--
Bend1a	100-L	4-pt bend	A-M compression	700 N	28 Nm
Bend1b	100-L	4-pt bend	A-M tension	700 N	28 Nm
Ax2a	91-R	Axial load	Knee fully flexed	1260 N	--
Ax2b	91-R	Axial load	Knee flexed 90°	766 N	--
Bend2a	91-R	4-pt bend	A-M compression	700 N	21 Nm
Bend2b	91-R	4-pt bend	A-M tension	700 N	21 Nm

Each specimen was instrumented with three (3) strain gauge rosettes (CAE-06-062UR-350, Measurement Group, Inc., Raleigh, NC). First, a 10 cm incision was made along the skin overlaying the mid-diaphyseal portion of the anterior tibial ridge. Next, two 5 cm transverse incisions were made at the proximal and distal ends of the first incision to create skin flaps. The fascia was cut away from the bone surface to expose the tibia. The periosteum was scraped off a small area (approximately 2 cm x 2 cm) of bone on the anteromedial, anterolateral, and posterior faces of the tibia, and these areas were dried with ether. A strain gauge rosette was then affixed to each of these surfaces using a cyanoacrylate adhesive. The fibula was left intact and was not instrumented.

Each specimen was subjected to two (2) axial compression tests using a Tinius Olson Locap Universal Test Machine (Willow Grove, PA) (Figure 1a). The foot was potted in a 30 cm x 15 cm x 8 cm box using Plaster of Paris. The heel was potted below the level of the malleoli so as not to constrain their motion. The foot box was secured to the frame of the test machine with clamps, and the knee was strapped to a steel plate that was curved to roughly conform to the surface of the distal thigh. The leg was aligned as vertically as possible and then compressed axially at a rate of 10 mm/min up to a maximum load of 2000 N. It was noted that the knee was forced into full flexion (> 135°) during axial compression. Therefore, a second axial compression test was performed on each specimen with the femur stump strapped tightly to the compression plate in order to fix the knee angle near ninety degrees (90°).

After the axial compression tests, the tibia was excised from the rest of the leg. Care was taken to preserve the attachments of the strain gauges. Each tibia was subjected to two (2) four-point bending tests up to a maximum load of 700 N at a rate of 10 mm/min (Figure 1b). The maximum moment experienced at the midshaft of the bone was 28 Nm. The lower supports were spaced 24 or 28 cm apart (d_{lower}), and the upper supports were spaced 12 cm apart (d_{upper}). The externally applied moment (M_{ext}) experienced by the midshaft of the tibia in between the upper supports was calculated based on the external force (P) applied by the test machine to the upper supports:

$$M_{ext} = P \cdot \left(\frac{d_{lower} - d_{upper}}{4} \right) \tag{1}$$

The upper support was hinged about its center to ensure that equal loading was applied by each support. In the first bending test, the anteromedial surface of the tibia faced upwards and was subjected to compression. In the second test, the tibia was flipped over so that anteromedial surface faced downwards and was subjected to tension. All tests were non-injurious.
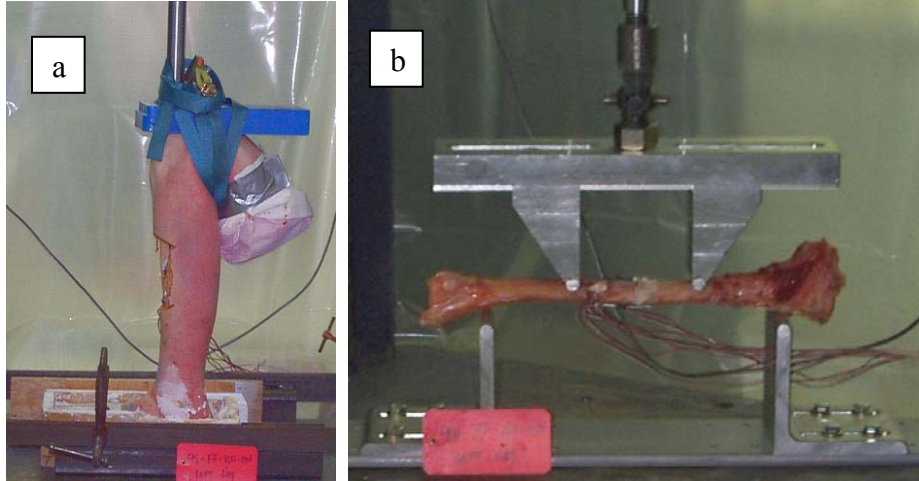
Figure 1: a) Axial compression test (Ax1a), and b) four-point bending test (Bend1b).

Data Processing

Geometric properties and the locations of the strain gauges on the tibial cross-section were obtained from computed tomography (CT) scans of the instrumented tibias taken after testing was complete. The resolution of the scans was 0.3125 mm/pixel and the slice thickness was 10 mm. The CT image data were converted into ASCII files using a custom-written Matlab program. The image data consisted of the coordinates of each pixel and the grayscale value. Pixels having a grayscale value above a certain threshold were considered to represent cortical bone. The exact threshold value was selected by trial and error until the thresholded image appeared, in our judgment, to be a good representation of the original image (Figure 2). Geometric properties of the thresholded cross-section were calculated using a custom FORTRAN program. The data were analyzed using the coordinate system of the CT image. The coordinates of the middle strain gauge of each rosette were determined from the locations of the wires on the CT images. The CT coordinate frame was related to the anatomical frame based on the position of the tibias in the CT scanner. In this study, the tibias were placed on the posterior protrusions of the femoral condyles in good alignment with the scanner. Therefore, the anterior direction coincided with the –Y axis direction in the CT frame, and the medial direction coincided with the +X axis of the CT frame for the right leg, and the –Y axis for the left leg (Figure 2).

Geometric parameters were calculated using standard equations. First, the coordinates of the area centroid of the cross-section (x_{cg}, y_{cg}) were calculated:

$$x_{cg} = \frac{\sum_i x_i}{A}, \quad y_{cg} = \frac{\sum_i y_i}{A} \tag{2}$$

where x_i and y_i were the x- and y-coordinates of each thresholded point i, and A was the cross-sectional area of the threshold image. Once the location of the area centroid was determined, all coordinates were shifted such that the area centroid of the cross-section was at the origin. The moments of inertia I_{xx}, I_{yy}, and I_{xy} were then calculated:

$$I_{xx} = \frac{A}{12} + \sum_i y_i^2 \tag{3a}$$

$$I_{yy} = \frac{A}{12} + \sum_i x_i^2 \tag{3b}$$

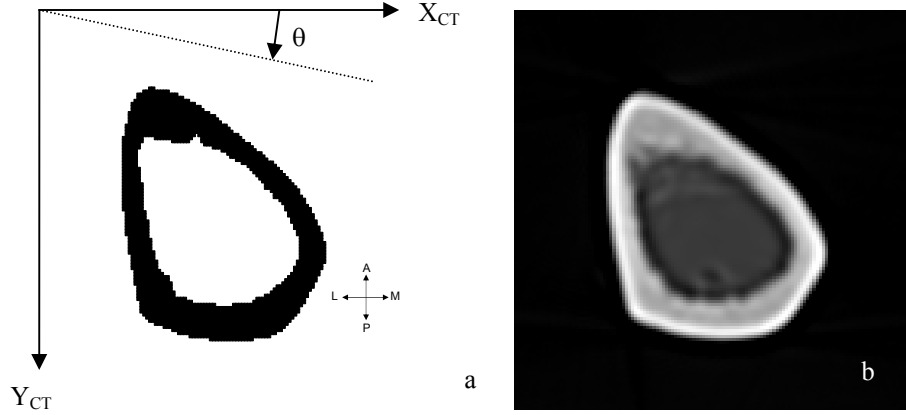$$I_{xy} = \sum_i x_i y_i \tag{3c}$$

Figure 2: Thresholded CT image of 91-R (a) shown alongside the original image (b).

The principal moments of inertia I_X and I_Y and the principal axis (θ_p) were then calculated:

$$I_X = \frac{I_{xx} + I_{yy}}{2} + \sqrt{\left(\frac{I_{xx} - I_{yy}}{2}\right)^2 + I_{xy}^2} \tag{4a}$$

$$I_Y = \frac{I_{xx} + I_{yy}}{2} - \sqrt{\left(\frac{I_{xx} - I_{yy}}{2}\right)^2 + I_{xy}^2} \tag{4b}$$

$$\theta_p = \frac{1}{2} \tan^{-1}\left(\frac{-2I_{xy}}{I_{xx} - I_{yy}}\right) \tag{4c}$$

Each strain gauge rosette consisted of three strain gauges numbered 1, 2, and 3. The configuration was a common one, such that gauge 2 was in the middle and oriented longitudinally on the bone, gauge 1 was to the left and oriented 45° clockwise, and gauge 3 was to the right and oriented 45° counterclockwise. For each strain gauge rosette, principal strains were calculated using standard equations (Higdon, 1985):

$$\varepsilon_P, \varepsilon_Q = \frac{\varepsilon_1 + \varepsilon_3}{2} \pm \sqrt{\frac{(\varepsilon_2 - \varepsilon_1)^2}{2} + \frac{(\varepsilon_2 - \varepsilon_3)^2}{2}} \tag{5a}$$

$$\theta_P = \frac{1}{2} \tan^{-1}\left(\frac{\varepsilon_1 - \varepsilon_3}{\varepsilon_1 + \varepsilon_3 - 2\varepsilon_2}\right) \tag{5b}$$

where ε_P was principal longitudinal strain, ε_Q was the principal transverse strain, and θ_P was the angle of P with respect to the longitudinal axis of gauge 2. The ratio of Q/P was calculated by fitting a line to the parametric plot of ε_Q vs. ε_P. In subsequent equations, the strain ε_i for each rosette i is understood to mean the principal longitudinal strain ε_P.

The location of the neutral axis was determined at each time point using the strain gauge data. Based on the assumption that plane sections remain plane, a linear strain profile was assumed to exist across the cross-section. The coordinates of points of zero strain (x^0_{ij}, y^0_{ij}) were calculated by linear interpolation of the strain gauge data:

$$x^0_{ij} = x^g_i - \left(\frac{\varepsilon_i}{\varepsilon_j - \varepsilon_i}\right)\left(x^g_j - x^g_i\right) \tag{6a}$$

$$y^0_{ij} = y^g_i - \left(\frac{\varepsilon_i}{\varepsilon_j - \varepsilon_i}\right)\left(y^g_j - y^g_i\right) \tag{6b}$$

where (x^g_i, y^g_i) and (x^g_j, y^g_j) were the coordinates of the center strain gauges on rosettes i and j. Points of zero strain were calculated for all combinations of rosette locations. The neutral axis was then obtained by fitting a line through the points of zero strain. In this study, strain was measured at only three locations, so although three points of zero strain could be calculated, one of these points was the result of redundant equations. Therefore, it was not necessary to perform a least-squares fit through the three points because a perfect fit could be obtained by connecting a line between any two of the three points:

$$m_{N/A} = \frac{y^0_{ij} - y^0_{jk}}{x^0_{ij} - x^0_{jk}} \tag{7a}$$

$$b_{N/A} = y^0_{ij} - m_{N/A} x^0_{ij} \tag{7b}$$

where $m_{N/A}$ and $b_{N/A}$ are the slope and y-intercept, respectively, of the neutral axis. The location of the neutral axis could alternatively be expressed by the angle of the neutral axis ($\theta_{N/A}$) in the CT coordinate frame and the perpendicular distance ($d_{N/A}$) from the neutral axis to the area centroid of the cross-section (located at the origin):

$$\theta_{N/A} = \tan^{-1} m_{N/A} \tag{8a}$$

$$d_{N/A} = \frac{-b_{N/A}}{\sqrt{m^2_{N/A} + 1}} \tag{8b}$$

Once the location of the neutral axis was determined, the value of the moment of inertia about the neutral axis ($I_{N/A}$) and the angle of the applied moment (θ_M) were determined:

$$I_{N/A} = \frac{I_X + I_Y}{2} + \frac{I_X - I_Y}{2} \cos(2\theta_{N/A} - 2\theta_p) \tag{9}$$

$$\theta_M = \theta_p + \tan^{-1}\left[\frac{I_Y}{I_X} \tan(\theta_{N/A} - \theta_p)\right] \tag{10}$$

It was sometimes necessary to add or subtract 180° from the value of θ_M calculated in eq. (10) to ensure that θ_M reflected the appropriate direction of bending. In the four-point bend tests, the applied moment was known from eq. (1) and it was desired to determine the Young's modulus (E) of the bone. First, the component of the external moment that was applied about the neutral axis ($M_{N/A}$) was calculated:

$$M_{N/A} = M_{ext} \cos(\theta_{N/A} - \theta_M) \tag{11}$$

Next, the perpendicular distance from each rosette to the neutral axis (c_i) was calculated:

$$c_i = \frac{-m_{N/A} xg_i + yg_i - b_{N/A}}{\sqrt{m^2_{N/A} + 1}} \tag{12}$$

where (xg_i, yg_i) were the coordinates of rosette i.

The maximum strain (ε_{max}) experienced in the tibial cross-section was calculated by finding the furthest distance (c_{max}) between any point on the periosteal surface and the neutral axis using the same formula as eq. (12), then linearly scaling up the strain measured at the nearest rosette i:

$$\varepsilon_{max} = \frac{c_{max}}{c_i} \varepsilon_i \tag{13}$$

The stress experienced at each rosette location was calculated using linear beam theory:

$$\sigma_i = \frac{M_{N/A} c_i}{I_{N/A}} \tag{14}$$

The stress and strain experienced at the location of each rosette at each time point were then plotted parametrically, and a line was fit through the data. The slope of the line was reckoned to be the Young's modulus (E) of the bone:

$$E = \frac{\sigma}{\varepsilon} \tag{15}$$

Eq. (15) assumes that bone can be modeled as a linear elastic material.

The Young's modulus was alternatively calculated based on the deflection (δ) of the bone at the location of the upper support, which corresponded to the vertical displacement y(a) of the crosshead of the test machine:

$$\delta = y(a) = \frac{Pa^2}{12E_\delta I_{N/A}}(4a - 3L)\cos^2(\theta_{N/A} - \theta_M) \tag{16}$$

where a was the horizontal distance between the upper and lower supports (6 cm or 8 cm), L was the horizontal distance between the lower supports, and P was the total crosshead load applied to both upper supports. The crosshead load, scaled according to eq. (16), was plotted parametrically against the crosshead displacement, and the slope of that line was reckoned to be the Young's modulus of the bone, denoted here as E_δ. Eq. (16) assumes that bone is a linear elastic material, the bone structure is prismatic, and deflection due to shear loading can be neglected.

Once the Young's modulus was determined for each specimen based on the four-point bending tests, the loads and moments experienced by the tibia in the axial loading tests were calculated. In the axial loading tests, the location of the neutral axis was calculated using eq.'s (6 – 10), just as was done in the four-point bending tests. The resultant bending moment (equivalent to M_{ext}) was then calculated by combining eq.'s (11), (14), and (15):

$$M_{res} = \frac{E\varepsilon_i I_{N/A}}{c_i \cos(\theta_{N/A} - \theta_M)} \tag{17}$$

Because strains were measured at only three locations in this study, eq. (17) yielded the same result for each rosette i.

In order to calculate the axial load, it was necessary to decompose the strain recorded at each rosette into the component that was due to pure axial loading and the component that was due to bending. The strain component due to pure axial loading (ε_{axial}) was assumed to be equal at all three locations. When the axial component is subtracted from the strain measured at each rosette, the remaining strain levels correspond to pure bending. In pure bending, the neutral axis should theoretically pass through the centroid of the cross-section. Therefore, the level of strain that, when subtracted from each measured strain, caused the recalculated neutral axis to pass through the area centroid was determined to be the strain component due to pure axial loading. Because strains were measured at only three locations in this study, it was possible to derive a simple closed-form expression by combining eq. (6a) and eq.'s (7a, b):

$$\varepsilon_{axial} = \varepsilon_i + (\varepsilon_j - \varepsilon_i)\frac{m_{N/A}x_i^g - y_i^g}{m_{N/A}x_i^g - y_i^g - m_{N/A}x_j^g + y_j^g} \tag{18}$$

The component of the maximum strain that was due to bending (ε_{bend}) was compared to the axial strain component by calculating a simple ratio:

$$\frac{\varepsilon_{bend}}{\varepsilon_{axial}} = \frac{\varepsilon_{max} - \varepsilon_{axial}}{\varepsilon_{axial}} \tag{19}$$

The axial load in the tibia was then calculated:

$$Tib\ F_z = EA\varepsilon_{axial} \tag{20}$$

In keeping with standard sign convention, both ε_{axial} and Tib F_z were negative in compression. The Young's modulus (E) derived from the strain gauge data was used in the above calculation, because it was felt to be more accurate than the modulus derived from the crosshead displacement (E_δ). The percentage of the total load P that was borne by the fibula was estimated assuming the tibia and fibula were the only two compressive load paths in the leg:

$$Fib\ F_z(\%) = 1 - \frac{Tib\ F_z}{P} \tag{21}$$

In the above procedure, the location of the centroid was assumed to be known, and that information was used to calculate the axial load experienced by the bone. In order to investigate the possibility that the effective centroid of the bone cross-section was not at the same location as the area centroid determined from the CT data (eq. 2), this procedure was reversed. The axial load in the tibia was assumed to be known, which allowed the two axial loading tests for each specimen to be treated as calibration tests in order to determine the location of the effective centroid. For each axial loading test, a sensitivity analysis was performed to evaluate the relationship between the distance over which the neutral axis is shifted and the calculated axial load (eq. 20). The distance necessary to shift the neutral axis such that the calculated axial load level (Tib F_z) was 90% of the crosshead load P was determined. The intersection of the shifted neutral axes for both axial load tests (knee fully flexed and knee flexed 90°) of each specimen was defined as the effective centroid of the cross-section.

In order to calculate the location of the axial load path relative to the tibial diaphysis, the tibia was assumed to be loaded by a purely axial eccentric load. Using the effective centroid in which the calculated Tib F_z was 90% of the crosshead load, the coordinates of that eccentric load (x_e, y_e) were calculated:

$$x_e = -\frac{M_{res} \sin \theta_M}{Tib \ F_z} \tag{22a}$$

$$y_e = \frac{M_{res} \cos \theta_M}{Tib \ F_z} \tag{22b}$$

Values for x_e and y_e were obtained from the slope of a regression line fit to the parametric plot of moment component vs. axial force. In order to contextualize the location of the calculated centers of pressure, a view of the leg along the Z-axis was constructed. Outlines of the tibial plateau and tibial plafond were traced from the CT scans, and the location of their area centroids were calculated. The direction of the long axis of the tibia was defined by the line connecting the area centroids of the tibial plateau and the tibial plafond. The outlines of the tibial plateau and tibial plafond were then overlaid on the thresholded image of the midshaft of the tibia such that the long axis of the tibia was perpendicular to the cross-sections. This procedure corrected for the slight misalignment of the tibias in the CT scanner and produced an image overlay of a tibia that was perfectly aligned along its long axis.

RESULTS

Geometric data obtained from the post-test CT scans demonstrated that the midshaft tibial cross-sections were oblong and asymmetric, with the bones being wider along the A-P axis than the M-L axis (Table 3). The cross-sections were generally oriented with the widest portion of the bone parallel to the anteromedial face (Figure 2). Strain gauge data were successfully collected in every test (Table 4). In some tests, one of the side gauges on a rosette failed (gauge 1 or gauge 3). In these tests, it was not possible to calculate the transverse principal strain ε_Q and the angle of the principal strain θ_p independently, and the principal strain was assumed to be the same as the strain measured by the longitudinal strain gauge (gauge 2). With the exception of the anteromedial rosette in the axial loading tests with the knee fully flexed, the angle of the principal strain on every rosette in all tests was within 13° of the longitudinal axis of the rosette. This was felt to be within the tolerance associated with mounting the rosettes to the bone by hand. In the axial loading tests with the knee fully flexed, the neutral axis passed very near the center gauge on the anteromedial rosette. It was felt that the larger θ_p values in those cases was not due to torsion, but rather that it was an artifact of the spacing between the gauges on the rosette, which placed one of the side gauges in tension and the other in compression. Therefore, it was concluded that the principal strains experienced by the bone in all tests were oriented predominantly along the long axis of the tibia, which was consistent with the strains being produced by axial loading and bending, rather than shear and torsion. The maximum strain in any test was -1810 $\mu\varepsilon$, which is well below the expected longitudinal yield strain for cortical bone of approximately -6000 $\mu\varepsilon$ (Burstein et al., 1976; Funk et al., 2004a). The maximum strain measured at any of the gauge locations underestimated the true maximum strain in the cross-section by 0% – 46% (Table 4).

Table 3. Midshaft Cross-Sectional Geometric Properties
Of Each Specimen Obtained From Post-Test CT Scans.

Specimen ID	Area (cm^2)	I_{xx} (cm^4)	I_{yy} (cm^4)	I_{xy} (cm^4)	I_X (cm^4)	I_Y (cm^4)	θ_p (deg)	$I_{A-P\ axis}$ (cm^4)	$I_{M-L\ axis}$ (cm^4)
100-L	2.95	2.29	1.48	-0.66	2.65	1.11	-61	1.48	2.29
91-R	1.90	1.21	0.84	0.29	1.36	0.68	62	0.84	1.21

Table 4. Summary Of Strain Gauge Data For Each Test.

Test name	Anteromedial rosette			Anterolateral rosette			Posterior rosette			ε_{max} ($\mu\varepsilon$)
	ε_P ($\mu\varepsilon$)	$\varepsilon_Q/\varepsilon_P$	θ_P (deg)	ε_P ($\mu\varepsilon$)	$\varepsilon_Q/\varepsilon_P$	θ_P (deg)	ε_P ($\mu\varepsilon$)	$\varepsilon_Q/\varepsilon_P$	θ_P (deg)	
Ax1a	-143	-.53	25	345	-.26	-6	-1038	n/a	n/a	-1514
Ax1b	380	n/a	n/a	-236	-.47	-12	-1086	n/a	n/a	-1086
Bend1a	-959	-.35	-5	771	-.20	11	864	n/a	n/a	1213
Bend1b	1235	-.35	-3	-896	-.20	13	-988	n/a	n/a	-1426
Ax2a	118	-.63	22	245	-.03	3	-1480	.07	-4	-1810
Ax2b	332	-.42	0	-305	-.33	-9	-918	.04	-3	-923
Bend2a	-1119	-.40	0	942	-.30	-6	1158	-.21	0	1519
Bend2b	1334	-.40	1	-1016	-.35	-12	-1119	-.11	10	-1570

Although the first leg specimen (100-L) was successfully tested twice in axial compression up to a load of 2000 N, the second leg specimen (91-R) appeared to yield at approximately 1200 N in the first axial compression test, and at approximately 700 N in the second axial compression test (Table 1). When the tibia was excised and inspected in preparation for the four-point bending tests, no damage could be found anywhere on the bone. Therefore, it was assumed that the apparent yielding in the axial compression tests was due to either slippage of the specimen or failure at some other anatomic location, such as the femoral condyles or the calcaneus. There was no observed specimen slippage or apparent yielding in any of the tibial four-point bending tests.

The location of the neutral axis changed very little during the time course of each test, so its location at the time of peak loading was selected to represent the entire test. In the four-point bending tests, the moment was generally applied about an axis parallel to the broad anteromedial face of the bone that rested on the supports. In these tests, the neutral axis and moment axis were near to each other and to the principal axis of inertia (Table 5). The neutral axis passed very close to the area centroid in all of the four-point bending tests. When the direction of bending was reversed on the same bone, the neutral axis shifted approximately 0.5 mm towards the side of the bone that was in compression.

Table 5. Summary Of Bending Test Results.

Test name	$\theta_{N/A}$ (deg)	$d_{N/A}$ (mm)	θ_M (deg)	E (GPa)	E_δ (GPa)
Bend1a	-58	0.0	-44	22.4	10.3
Bend1b	121	-0.4	123	22.0	11.8
Bend2a	53	-0.6	46	22.9	9.8
Bend2b	-123	-0.1	-128	21.1	11.6

For each bending test, a linear relationship was observed between the stress and strain experienced at the location of each strain gauge rosette (Figure 3). Furthermore, the slope of that line was consistent for each rosette in a given test. This calculated Young's modulus (E) of the bone was similar for each specimen, but tended to be slightly higher for the four-point bending tests in which the anteromedial face of the tibia was in compression as opposed to tension. The Young's modulus calculated using the strain gauge data (E) was approximately twice as high as the modulus calculated using the crosshead displacement data (E_δ). The

Young's modulus calculated from displacement (E_δ) tended to be slightly higher for four-point bending tests in which the anteromedial face of the tibia was in tension as opposed to compression.
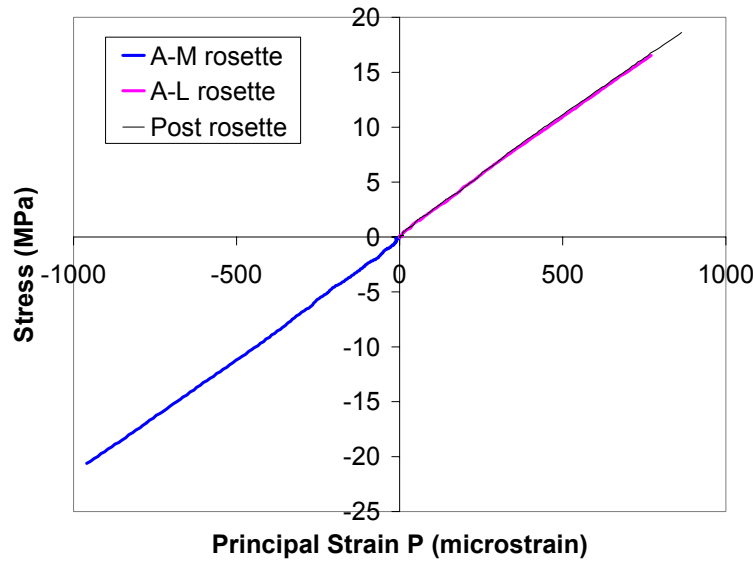

Figure 3: Parametric stress-strain plots for Bend1a.

For the axial compression tests, the induced bending moment and axial force was calculated using the average Young's modulus (E) obtained from the two four-point bending tests on the same specimen. The magnitude of the bending moments induced in the axial compression tests were comparable to or greater than the moments applied in the four-point bending tests. The angle of the knee had a pronounced effect on the direction of bending induced in the tibia. When the knee was fully flexed, the induced moment was about an axis about 25° posterior to pure lateral. When the knee angle was fixed at 90°, the induced moment was about an axis that was almost purely lateral (Table 6). The effect of knee angle on the orientation of the neutral axis was even greater, due to the asymmetry of the bone cross-section (Figure 4).
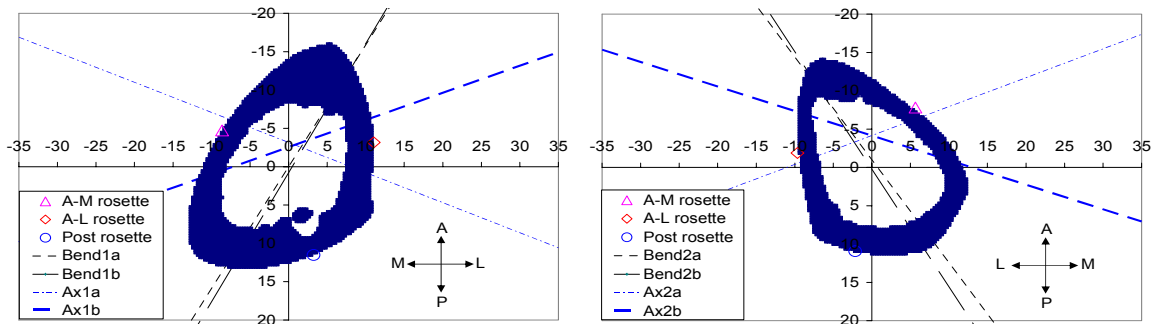

Figure 4: Location of the neutral axis in all tests.

Table 6. Summary Of Axial Compression Test Results Using Area Centroid.

Test name	$\theta_{N/A}$ (deg)	$d_{N/A}$ (mm)	θ_M (deg)	M_{res} (Nm)	Tib F_z (N)	Fib F_z (%)	ε_{axial} ($\mu\varepsilon$)
Ax1a	-159	2.9	-155	49	-1593	20%	-243
Ax1b	161	2.4	176	36	-1173	41%	-179
Ax2a	159	3.9	158	35	-1856	-47%	-433
Ax2b	-162	4.0	-177	16	-1048	-37%	-244

Table 7. Summary Of Axial Compression Test Results Using Effective Centroid.

Test name	$\theta_{N/A}$ (deg)	$d_{N/A}$ (mm)	θ_M (deg)	M_{res} (Nm)	Tib F_z (N)	Fib F_z (%)	$x_{eff\ cent}$ (mm)	$y_{eff\ cent}$ (mm)	x_e (mm)	y_e (mm)	ε_{axial} ($\mu\varepsilon$)	ε_{bend} / ε_{axial}
Ax1a	-159	3.3	-155	49	-1800	10%	1.2	0.9	-12	24	-275	4.5
Ax1b	161	3.6	176	36	-1800	10%			1	18	-275	3.0
Ax2a	159	2.4	158	35	-1134	10%	-0.6	-1.5	13	28	-264	5.9
Ax2b	-162	2.8	-177	16	-690	10%			1	21	-161	4.7

The calculated axial tibial loads did not appear to be realistic in any of the tests when calculated using the area centroid as determined from CT scans. The calculated tibial load was lower than expected for specimen 100-L, but higher than expected for specimen 91-R. The calculated tibial load was also much greater in tests with the knee fully flexed as opposed to fixed at 90°. A sensitivity analysis demonstrated that the calculated tibial axial load was very sensitive to the distance over which the neutral axis was shifted (Figure 5). The level of axial strain ε_{axial} necessary to shift the neutral axis 1 mm corresponded to a calculated tibial axial load equal to 25% – 40% of the crosshead load. The component of the maximum strain that was due to bending was 3 – 6 times higher than the component due to axial loading (Table 7). The distance from the neutral axis to the area centroid of the cross-section was greater in specimen 91-R than specimen 100-L, but the reverse was true when considering the effective centroid (Table 7). The distance from the neutral axis to the effective centroid was greater in tests with the knee fixed at 90° as opposed to fully flexed. In both specimens, the effective centroid was about 1.5 mm away from the area centroid, but not in a consistent direction. In specimen 100-L, the effective centroid was medial and posterior to the area centroid, and in specimen 91-R, the effective centroid was medial and anterior to the area centroid. The estimated location of the eccentric axial load was similar in both specimens. The estimated distance from the eccentric load to the effective centroid was larger when the knee was fully flexed as opposed to being fixed at 90°. In all the four axial compression tests, the eccentric load appeared to be applied to a point outside of the mid-diaphyseal bone cross-section (Figure 6).
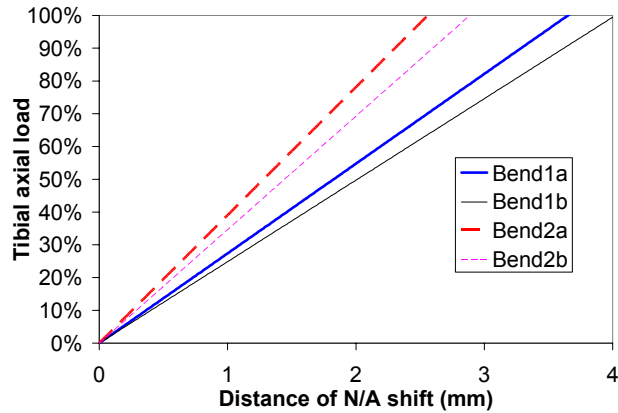

Figure 5: Sensitivity of the calculated tibial axial load (as a percentage of the crosshead load) to the distance over which the neutral axis was shifted.
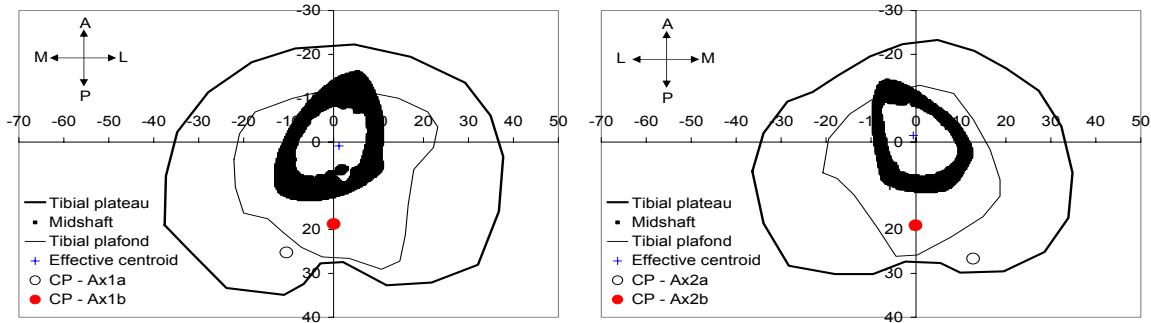
Figure 6: Location of effective centroid and calculated centers of pressure (CP). The long axis of the tibia connecting the area centroids of the tibial plateau and the tibial plafond is perpendicular to the cross-sections. The origin is still the area centroid of the tibial diaphysis.

DISCUSSION

The purpose of this pilot study was to evaluate the effectiveness and limitations of using linear beam theory to calculate the loads and moments experienced by the human tibia based on *in vitro* strain measurements. The loading condition studied was pure axial compression of the leg with the ankle neutrally positioned and the knee flexed. The degree of load sharing between the tibia and fibula in this loading configuration has been studied extensively using both strain gauges and *in situ* load cells. These two instrumentation techniques have yielded divergent results. Strain gauge studies have reported that the fibula bears anywhere from 5% (Segal et al., 1981) to 17% (Lambert, 1971; Wang et al., 1996) of the total leg load, while studies that have implanted load cells in both the tibia and fibula have consistently reported that the fibula bears only about 7% of the axial load in the leg (Takebe et al., 1984; Goh et al., 1992; Funk et al., 2004b).

It is difficult to evaluate the results of previous strain gauge studies on this topic, because most published reports have not documented the methodology used to calculate axial loads from the strain gauge data (Lambert, 1971; Segal et al., 1981; Skraba and Greenwald, 1984; Thomas et al., 1995). Only Wang et al. (1996) have documented their attempts to calculate axial loads using beam theory. They applied a simplified model in which the tibial and fibular diaphyses were considered to be subject to purely centered axial loading without bending. This approach was justified by their finding that axial loading of the leg produced uniform compressive strains around the perimeter of the cross-section in both the tibia and the fibula. However, this finding is contradicted by the present study and by other studies (Skraba and Greenwald, 1984; Thomas et al., 1995), which have all reported that when the leg is axially loaded, one side of the tibia goes into tension and the other side goes into compression. Therefore, the basis for axial load sharing calculations of Wang et al. (1996) must be considered invalid and the results erroneous.

The quality of the data obtained from strain gauge studies of long bones can be significantly enhanced by applying linear beam theory as outlined in the present study. If strains are measured at three locations or more, it is possible to evaluate bone strains not only at discrete locations, but at any point in the cross-section. Complete characterization of the strain field in a cross-section can provide considerably more information than strain measurements at discrete locations. For example, in the present study, strains at the gauge locations underestimated the peak strains in the cross-section by up to 46%, depending on the orientation of the neutral axis (Table 4). Linear beam theory can also be used to calculate the internal loads and moments experienced by the bone, which are often the parameters of greatest interest. These calculations require the assumption that bone can be modeled as a homogeneous, linear elastic material, but do not require the assumption that the bone structure is prismatic.

An engineering analysis can additionally determine the location of the axial load path in a long bone. This calculation was performed in the present study by assuming that the tibia was loaded in pure eccentric compression (eq. 22). This assumption implies that there is no ligament tension at the knee or ankle, because ligament tension combined with joint compression will create a bending couple. We believe this assumption probably is valid when the knee is flexed 90 degrees. However, when the knee is forced into maximal flexion, there is likely to be tension in the cruciate ligaments of the knee. This additional bending couple at the knee may have caused the calculated centers of pressure in tests Ax1a and Ax2a to be further

from the centroid than the actual compressive centers of pressure. In tests with the knee flexed 90 degrees (Ax1b and Ax2b), the eccentric axial load path was calculated to pass approximately 20 mm posterior to the centroid of the tibial diaphysis, which is well outside of the cross-section (Figure 6). This is possible because the tibial plateau has a much larger cross-sectional area than the mid-diaphysis and extends quite a bit posteriorly.

The results of the present study suggest that the application of linear beam theory to *in vitro* tibial strain gauge data in this loading configuration is likely to produce erroneous results when calculating the axial load. We attribute this error to the following three factors, listed in order of importance: the curved geometry of the tibia, the inhomogeneity of the diaphyseal cross-section, and a mild nonlinearity of the bone material in tension vs. compression. Results from the present study support the use of a linear elastic material model overall (Figure 3). Obviously, this conclusion rests on the assumption that the maximum bone strain is always below the yield point. Also, the evaluation of linear beam theory was limited to the study of longitudinal strain in the present study; strains due to shear loading or torsion were not addressed. The specific material nonlinearity of bone that may be of importance in this study is the fact that bone has been reported to be roughly 10% stiffer in compression than in tension (Burstein et al., 1976). In a perfectly linear material, the neutral axis would be expected to always pass through the centroid in pure bending, regardless of direction. In the present study, the neutral axis shifted approximately 0.5 mm towards the side of the tibia that was in compression in four-point bending tests on the same bone when the direction of bending was reversed. This distance is consistent with the bone material being approximately 10% stiffer in compression than in tension. Another possible explanation for the shift in the neutral axis towards the compressive side of the bone is that the tibial diaphysis was also subjected to tension during the four-point bending tests. However, we believe that the level of tension in the bone would have been low due to the slippery interface between the bone and the supports. A mild nonlinearity in bone stiffness in tension vs. compression could be expected to change the location of the effective centroid slightly as a function of the direction of bending. Therefore, the location of the effective centroid might not be a fixed point in the tibial cross-section, but rather a point that can move within a cloud having a 0.5 mm diameter.

Additional error in applying linear beam theory to the diaphysis of a bone is created by the assumption that the entire cross-section consists of a uniform, homogeneous material. This assumption is implicit in the calculation of the area centroid and moments of inertia (eq.'s 2 – 4). However, visual inspection of the CT scan reveals evidence of some inhomogeneity in the cross-section of the tibial diaphysis, in that the cortical shell appears denser than the endosteal bone (Figure 2b). Carter et al. (1981) developed a method to account for cross-sectional bone inhomogeneity by running three calibration tests and using that data to solve a set of simultaneous equations. Their method calculated an effective centroid and an effective modulus based on area properties. That approach was shown to greatly improve the accuracy of the calculated axial load applied to an isolated canine radius. The present study applied an independently derived but similar methodology in order to calculate the location of the effective centroid in the human tibia. It was found that the effective centroid was located approximately 1.5 mm away from the area centroid in each of the two specimens tested.

The relatively small errors associated with deviations from the assumptions of linearity and homogeneity are amplified by the curved geometry of the human tibia when the axial load is calculated. Due to the curvature of the tibia, compression of the leg induces a large bending moment in the midshaft of the tibia. In fact, the strain due to bending was 3 – 6 times higher than the strain due to axial compression in the present study (Table 7). This creates what is fundamentally a signal-to-noise ratio problem when attempts are made to separate out the relatively small component of strain due to axial loading. Because of the large bending strains, the neutral axis passed very near the centroid of the diaphyseal cross-section (Figure 4). Therefore, a small error in the estimated location of the bone centroid resulted in a large error in the calculated axial load. Specifically, there was a 1.5 mm error associated with the location of the effective centroid, but the neutral axis passed only about 3 mm from the centroid, which resulted in errors of up to 50% in the calculated axial load (Tables 6 and 7). In a straight bone, the entire cross-section may be in compression such that the neutral axis passes entirely outside of the bone. Hypothetically, if the neutral axis had passed 30 mm away from the centroid, then the same 1.5 mm error in the location of the effective centroid would have resulted in only a 5% error in the calculated axial load. Therefore, the curvature of the tibia combined with errors in the engineering assumptions made it impossible to accurately calculate the axial load in the tibia in the present study.

Real long bones may be either curved or straight. The strain distribution in the tibia during gait has been shown to be dominated by bending in many animals, including horses (Hartman et al., 1984), dogs (Yoshikawa et al., 1994), sheep (Gautier et al., 2000), macaques (Demes et al., 2001), and humans (Goodwin and Sharkey, 2002). However, the role of bending has been shown to be minor in other bones, such as the canine radius (Carter et al., 1981), the horse metacarpus (Rybicki et al., 1977; Biewener et al., 1983; Gross et al., 1992), and the human first metatarsal (Goodwin and Sharkey, 2002). The present study is the first to our knowledge to report significant errors in calculating the axial load in a bone using strain gauge data. It may be that past successes in calculating axial bone loads from strain gauge data (Rybicki et al., 1977; Carter et al., 1981) have been assisted by a relatively straight bone geometry.

Of key importance in the discussion of error is the fact that the calculation of the bending moment is completely unaffected by any error associated with the calculation of the axial load (Table 7). The results of this study suggest that the bending moments experienced by the tibia can be accurately calculated from strain gauge data using linear beam theory (Figure 3). The bending moment calculation relies on accurate estimates of the elastic modulus and the geometric properties of the cross-section (eq. 17). Geometric properties of the bone cross-section derived from CT data can be highly dependent on the threshold value. This particular error was minimized in the present study by performing a four-point bending calibration test on the same bone with the strain gauges still in place. The modulus derived from the four-point bending test can be considered an effective modulus that accounts for errors in the calculated geometric properties. This approach is more accurate than simply assuming a value for the elastic modulus (Rybicki et al., 1977) or even conducting a test on a small sample from the specimen, which would not account for errors in geometric properties.

An incidental finding from the four-point bending tests was that the modulus calculated based on the load-deflection data was approximately half of the modulus calculated based on the strain gauge data, in spite of the fact that these two measurements are theoretically redundant (Table 5). Because the strain gauge provided a direct measurement of strain and deflection was only a surrogate measurement for strain, the moduli calculated from the strain gauge data were assumed to be more accurate. The finding that deflection data underpredict the modulus relative to strain gauge data has also been reported in three-point bending tests on cadaveric femurs (Funk et al., 2004a).

The results of the present study support the use of strain gauges to characterize the strain field and calculate the bending moment in the midshaft of a long bone. The strain gauge methodology is particularly valuable when implantation of a load cell is problematic, and the main loading parameter of interest is bending rather than axial load. We believe this methodology could be fruitfully applied to biomechanical experiments in which transverse loading is applied to a long bone, such as vehicle impacts into pedestrian lower extremities or airbag deployments involving an out-of-position upper extremity.

CONCLUSIONS

A detailed method was developed for applying linear beam theory to calculate the axial load and bending moments experienced by a long bone using strain gauge measurements taken at a minimum of three locations around the perimeter of an asymmetric cross-section. The method was applied to *in vitro* tibial strain measurements taken during axial compression tests of two cadaveric leg specimens in which the ankle was neutrally oriented and the knee was flexed. It was possible to calculate bending moments accurately, but not the axial loads. The estimated load-sharing by the fibula varied from -47% to 41%, which appears to be grossly in error. This error is attributed in large part to the curvature of the tibia, which causes a significant bending moment to be induced when the leg is subjected to pure axial compression. The axial load path passes approximately 20 mm posterior to the centroid of the tibial diaphysis, which is well outside of the cross-section. This large eccentricity in the axial load path creates strains due to bending that are 3 – 6 times higher than the strain due to axial loading. As a result, it is difficult to separate out the relatively small component of strain due to axial loading. Because the neutral axis passes very near the centroid of the cross-section (about 3 mm away in a bone having a diameter of approximately 25 mm), a small error in the estimated location of the bone centroid results in a large error in the calculated axial load. In this study, the effective centroid of the bones was estimated to be about 1.5 mm away from the area centroid. Although the large curvature of the tibia probably makes the calculation of axial loads from measured strains intractable, it is still possible to accurately calculate bending moments, which is useful for many applications (e.g., vehicle-

pedestrian tests). Also, the methodology presented here may be accurate when calculating the axial load experienced by bones that are straighter than the human tibia.

REFERENCES

BIEWENER, A. A., THOMASON, J., GOODSHIP, A., and LANYON, L. E. (1983). Bone Stress in the Horse Forelimb During Locomotion at Different Gaits: A Comparison of Two Experimental Methods. J Biomech, 16(8): 565 – 576.

BOURNE, R. B., FINLAY, J. B., PAPADOPOULOS, P., RORABECK, C. H., and ANDREAE, P. (1984). In Vitro Strain Distribution in the Proximal Tibia: Effect of Varus-Valgus Loading in the Normal and Osteoarthritic Knee. Clin Orthop Rel Res, 188: 285 – 292.

BURR, D. B., MILGROM, C., FYHRIE, D., FORWOOD, M., NYSKA, M., FINESTONE, A., HOSHAW, S., SAIAG, E., and SIMKIN, A. (1996). In Vivo Measurement of Human Tibial Strains During Vigorous Activity. Bone, 18(5): 405 – 410.

BURSTEIN, A. H., REILLY, D. T., and MARTENS, M. (1976). Aging of Bone Tissue: Mechanical Properties. J Bone Joint Surg, 58-A(1): 82 – 86.

CARTER, D. R., CALER, W. E., and HARRIS, W. H. (1981). Resultant Loads and Elastic Modulus Calibration of Long Bone Cross Sections. J Biomech, 14(11): 739 – 745.

DEMES, B., QIN, Y.-X., STERN, J. T., LARSON, S. G., and RUBIN, C. T. (2001). Patterns of Strain in the Macaque Tibia During Functional Activity. Am J Phys Anthrop, 116: 257 – 265.

EKENMAN, I., HALVORSEN, K., WESTBLAD, P., FELLANDER-TSAI, L., and ROLF, C. (1998). Local Bone Deformation at Two Predominant Sites for Stress Fractures of the Tibia: An In Vitro Study. Foot & Ankle Int, 19(7): 479 – 484.

FUNK, J. R., CRANDALL, J. R., TOURRET, L. J., MACMAHON, C. B., BASS, C. R., PATRIE, J. T., KHAEWPONG, N., and EPPINGER, R. H. (2002). The Axial Injury Tolerance of the Human Foot/Ankle Complex and the Effect of Achilles Tension. J Biomech Eng, 124(6): 1 – 8.

FUNK, J. R., KERRIGAN, J. R., and CRANDALL, J. R. (2004a). Dynamic Bending Tolerance of the Human Femur. Annual Proceedings of the Association for the Advancement of Automotive Medicine (AAAM), 48: 215 – 233.

FUNK, J. R., RUDD, R. W., KERRIGAN, J. R., and CRANDALL, J. R. (2004b). The Effect of Tibial Curvature and Fibular Loading on the Tibia Index. Traffic Injury Prevention, 5(2): 164 – 172.

GAUTIER, E., PERREN, S. M., and CORDEY, J. (2000). Strain Distribution in Plated and Unplated Sheep Tibia: An In Vivo Experiment. Injury, Int J Care Injured, 31: S-C37 – 44.

GOH, J. C. H., LEE, H., ANG, J., and PHO, R. W. H. (1992). Biomechanical Study on the Load-Bearing Characteristics of the Fibula and Effects of Fibular Resection. Clin Orthop Rel Res, 279: 223 – 228.

GOODWIN, K. J. and SHARKEY, N. A. (2002). Material Properties of Interstitial Lamellae Reflect Local Strain Environments. J Orthop Res, 20: 600 – 606.

GROSS, T. S., MCLEOD, K. J., and RUBIN, C. T. (1992). Characterizing Bone Strain Distributions *In Vivo* Using Three Triple Rosette Strain Gauges. J Biomech, 25(9): 1081 – 1087.

HARTMAN, W., SCHAMHARDT, H. C., LAMMERTINK, J. L. M. A., and BADOUX, D. M. (1984). Bone Strain in the Equine Tibia: An *In Vivo* Strain Gauge Analysis. Am J Vet Res, 45(5): 880 – 884.

HUISKES, R. (1982). On the Modeling of Long Bones in Structural Analyses. J Biomech, 15(1): 65 – 69.

KAJZER, J., SCHROEDER, G., ISHIKAWA, H., MATSUI, Y., and BOSCH, U. (1997). Shearing and Bending Effects at the Knee Joint at High Speed Lateral Loading. Society of Automotive Engineers, SAE Paper No. 973326, 151 – 165.

LAMBERT, K. L. (1971). The Weight-Bearing Function of the Fibula: A Strain Gauge Study. J Bone Joint Surg, 53A(3): 507 – 513.

LANYON, L. E., HAMPSON, W. G. I., GOODSHIP, E., and SHAH, J. S. (1975). Bone Deformation Recorded In Vivo from Strain Gauges Attached to the Human Tibial Shaft. Acta Orthop Scand, 46: 256 – 268.

RYBICKI, E. F., MILLS, E. J., TURNER, A. S., and SIMONEN, F. A. (1977). *In Vivo* and Analytical Studies of Forces and Moments in Equine Long Bones. J Biomech, 10: 701 – 705.

SHAABAN, H., GIAKAS, G., BOLTON, M., WILLIAMS, R., SCHEKER, L. R., and LEES, V. C. (2004). The Distal Radioulnar Joint as a Load-Bearing Mechanism – A Biomechanical Study. J Hand Surg, 29A(1): 85 – 95.

SEGAL, D., PICK, R. Y., KLEIN, H. A., and HESKIAOFF, D. (1981). The Role of the Interosseus Membrane on Tibiofibular Weightbearing. Foot & Ankle, 4(6): 301 – 304.

SKRABA, J. S. and GREENWALD, A. S. (1984). The Role of the Interosseus Membrane on Tibiofibular Weightbearing. Foot & Ankle, 4(6): 301 – 304.

TAKEBE, K., NAKAGAWA, A., MINAMI, H., KANAZAWA, H., and HIROHATA, K. (1984). Role of the Fibula in Weight-bearing. Clin Orthop Rel Res, 184: 289 – 292.

THOMAS, K A., HARRIS, M. B., WILLIS, M. C., LU, Y., and MACEWEN, G. D. (1995). The Effects of the Interosseus Membrane and Partial Fibulectomy on Loading of the Tibia: A Biomechanical Study. Orthopedics, 8(4): 373 – 383.

YOSHIKAWA, T., MORI, S., SANTIESTEBAN, A. J., SUN, T. C., HAFSTAD, E., CHEN, J., and BURR, D. B. (1994). The Effects of Muscular Fatigue on Bone Strain. J Exp Biol, 188: 217 – 233.

WANG, Q., WHITTLE, M., CUNNINGHAM, J., and KENWRIGHT, J. (1996). Fibula and Its Ligaments in Load Transmission and Ankle Joint Stability. Clin Orthop Rel Res, 330: 261 – 270.

DISCUSSION

PAPER: **Calculation of Long Bone Loading Using Strain Gauges**

PRESENTER: ***Dr. Jim Funk, Biodynamic Research Corporation and the University of Virginia Center for Applied Biomechanics***

QUESTION: *Guy Nusholtz, DaimlerChrysler*
You had a number of methods or a number of reasons why you didn't think you were getting good axial loads. Did you do any type of analysis to see … [whether or not] you had homogeneity? It seems to be there might be an actual instrumentation issue and you had nonlinearity. I would think you could test out nonlinearity by doing small changes in the actual loads to see if that was it. But, did you do any type of work to find out which of those was most important?

ANSWER: You can break it down and theoretically, the nonlinearity is not a very big issue. The inhomogeneity, I think, is probably the larger issue. We think the instrumentation is good because we have consistent results on both bones although having more strain gauges would be better just to verify that you are getting a good, accurate location at the neutral axis. I think the sensitivity analysis we did, which really lumps all that together, is really as far as we went, you know, trying to figure—All we know is that we don't have the exactly the right bone centroid and we looked at how far off we must have been.

Q: I guess, then, your basic conclusion is: There's no methodology that you could use which would correct it.

A: Well, there is. Dennis Carter developed a nice methodology. If you can take the bone out, pot it, apply, do some cantilever and bending at different angles—

Q: Okay.

A: You can do that, but it requires a good post-test calibration procedure, a lot more than we did in this particular test.

Q: Oh okay. So, there is a way to potentially recover.

A: Yes, if you can basically do a calibration procedure where you duplicate your loading, you can get loads and strains nicely correlated.

Q: So you could curve-fit this system?

A: You could bypass all that linear theory and go.

Q: That's right. You bypass everything. Okay.

A: Exactly.

Q: Thank you.

QUESTION: *Steve Rouhana, Ford Motor Company*
Jim, with regard to the homogeneity: Did you do cross-sectional microstructural analysis to see if the remodeling was similar in all areas of the bone and that could affect the properties?

A: Absolutely not.

Q: Okay. It's that a number of reversion systems around the bone can differ.

A: Right. Well, you can tell just, in fact, from looking at the CT scans that there's—That it doesn't even look homogeneous, you know. It's by—I think it was more towards the beginning of the thing, but— Oh. Here. You can definitely see an area that looks denser on the outer surface and kind of fuzzy area on the endosteal surface.

Q: Yeah. You might be able to correct that by looking at the porosity or the number of reversion system per cubic millimeter or something like that, per square millimeter.

A: That's a possibility, but we didn't go that far.

Q: Okay. Thanks.

QUESTION: *King Young, Wayne State University*
You know limited experience testing a tibia, we tend to find the specimen rotate during testing. Do you have that similar problem or have you encountered that?

A: We found that it did sort of immediately settle into a position and then it remained there, and our evidence for that is that the neutral axis location that we calculated stayed almost in exactly the same place throughout that bending test. So, we didn't really have a problem with the rotation.

Q: I see. What is your loading speed?

A: It was slow. Each of these tests probably took 10 seconds, something like that.

Q: I see. Actually, in our previous experience, we found the faster we load, the less rotation. The slower we load, the more rotation so maybe something we didn't do right.

A: Maybe we're just lucky.